Supporting Information

Versatile Interfacial Self-Assembly of $Ti_3C_2T_x$ MXene Based Composites with Enhanced Kinetics for Superior Lithium and Sodium Storage

Zhengguang Zou, Qian Wang, Jun Yan*, Kai Zhu, Ke Ye, Guiling Wang, Dianxue Cao*

Key Laboratory of Superlight Materials and Surface Technology, Ministry of Education, College of Materials Science and Chemical Engineering, Harbin Engineering University, Harbin 150001, China

*Corresponding authors.

Jun Yan, E-mail: yanjun198201@vip.163.com, yanjun@hrbeu.edu.cn

Qian Wang, E-mail: wangqianhrb@163.com

Content

EXPERIMENTAL

Chemicals. All the chemicals used in this work were of analytical grade and used as received without further purification. Ti_3AlC_2 was purchased from 11 Technology Co., Ltd (Jilin, China). Cyclohexane was Tianjin Fuyu Fine Chemical Co. Ltd (China). Concentrated hydrochloric acid (HCl), nickel chloride hexahydrate ($NiCl_2 \cdot 6H_2O$) and cobalt chloride hexahydrate ($CoCl_2 \cdot 6H_2O$) were obtained from Sinopharm Chemical Reagent Co. Ltd (China). *n*-dodecyl mercaptan ($C_{12}H_{26}S$), Oleylamine ($C_{18}H_{37}N$) and lithium fluoride (LiF) were purchased from Aladdin.

Preparation of MXene nanosheets. 2.5 mL of ultrapure water and 7.5 mL of hydrochloric acid were mixed and stirred for several minutes. Then 0.8 g of LiF was added. After 10 minutes later, 0.5 g of MAX (Ti_3AlC_2) was added slowly. Then, the mixed solution was transferred in water bath pot (40 ℃) for 36 hours. Then the obtained solution was washed and centrifuged (3500 rpm) with ultrapure water for several times. Sediment and 50 mL of ultrapure water was sonicated for 1 h with the protection of N_2 atmosphere. Then the mixed solution was centrifuged for 1 h. Finally, the MXene aqueous solution was obtained.

Structural characterization. X-ray diffraction patterns were charactered by Rigaku D/MAX-TTR III powder X-ray diffractometer with Cu Kα (λ = 0.15406 nm) radiation in the 2θ range of 5-80°. The XPS data was collected by a PHI 5700 ESCA X-ray photoelectron spectrometer with an Al Kα X-ray source. The morphology analysis of the materials was characterized by transmission electron microscope (TEM, FEI, Talos F200X G2). Fourier transform infrared (FT-IR) spectroscopy was carried out on a Perkin-Elmer 580B IR spectrophotometer using KBr pellets.

Electrochemical measurements. All electrochemical tests were conducted in CR2032 coin cells. For the preparation of anodes, active material (65 wt.%), super P (20 wt.%) and carboxymethyl cellulose (CMC, 15 wt.%) were mixed with deionized water in a mortar to make a homogeneous slurry, which was then uniformly coated onto a copper foil with a scraper and dried at 60 °C in a vacuum oven for at 24 h. The mass loading of active material was 1.5 mg cm^{-2} in each electrode.

For the assembly of Li-ion half cells, porous polypropylene film (Celgard 2400) was used as the separator and 1 M $LiPF_6$ dissolved in a mixture of ethylene carbonate/dimethyl carbonate/ethyl methyl carbonate (EC/DMC/EMC, 1:1:1, v/v/v) was used as the electrolyte. Coin cells were assembled with lithium metal sheet as the counter and reference electrodes in an argon-filled glove box (H_2O and O_2 < 0.01 ppm). All the electrode potential of the cells reported in this work is referred to the Li^+/Li reference electrode unless otherwise specified.

For the assembly of Na-ion half cells, glass fiber filters (Whatman GF/D) were used as the separator and 1 M $NaClO_4$ dissolved in a mixture of ethylene carbonate/dimethyl carbonate/ethyl methyl carbonate (EC/DMC/EMC, 1:1:1, Vol%) with 5.0% FEC was used as the electrolyte. Coin cells were assembled with sodium metal sheet as the counter and reference electrodes in an argon-filled glove box (H_2O and O_2 < 0.01 ppm). All the electrode potential of the cells reported in this work is referred to the Na^+/Na reference electrode unless otherwise specified.

Galvanostatic charge-discharge cycles were tested using a NEWARE battery testing system (CT-4008) at various current densities between 3 and 0.01 V at room temperature.

Cyclic voltammetry measurements were carried out on an electrochemical station (VMP3, Bio-Logic) within a potential window of 0.01-3 V. Electrochemical impedance spectra were analyzed on a VMP3 electrochemical station with the AC amplitude of 5 mV in the frequency range of 100 kHz to 0.01 Hz.

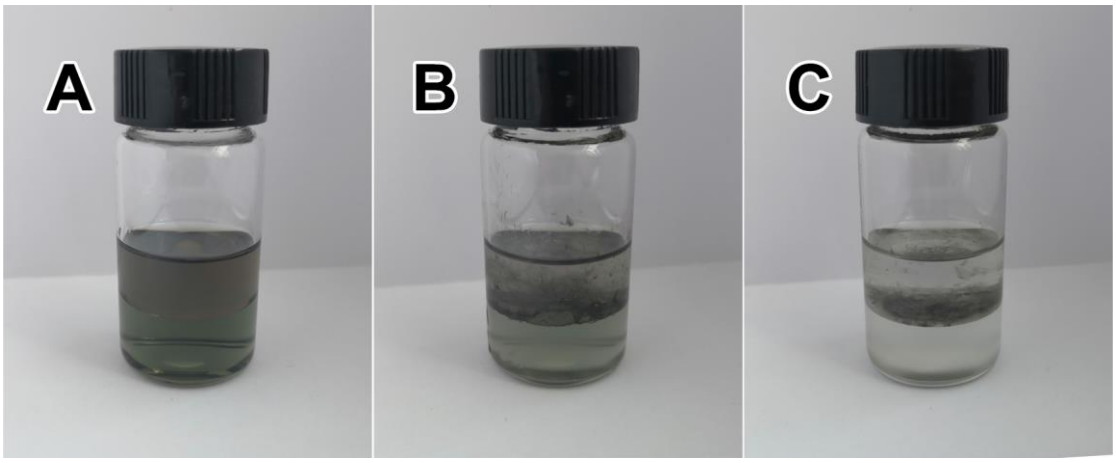

Figure S1. Optical images during the interfacial self-assembly process. (A) Before self-assembly. (B) Self-assembly in progress. (C) After self-assembly.

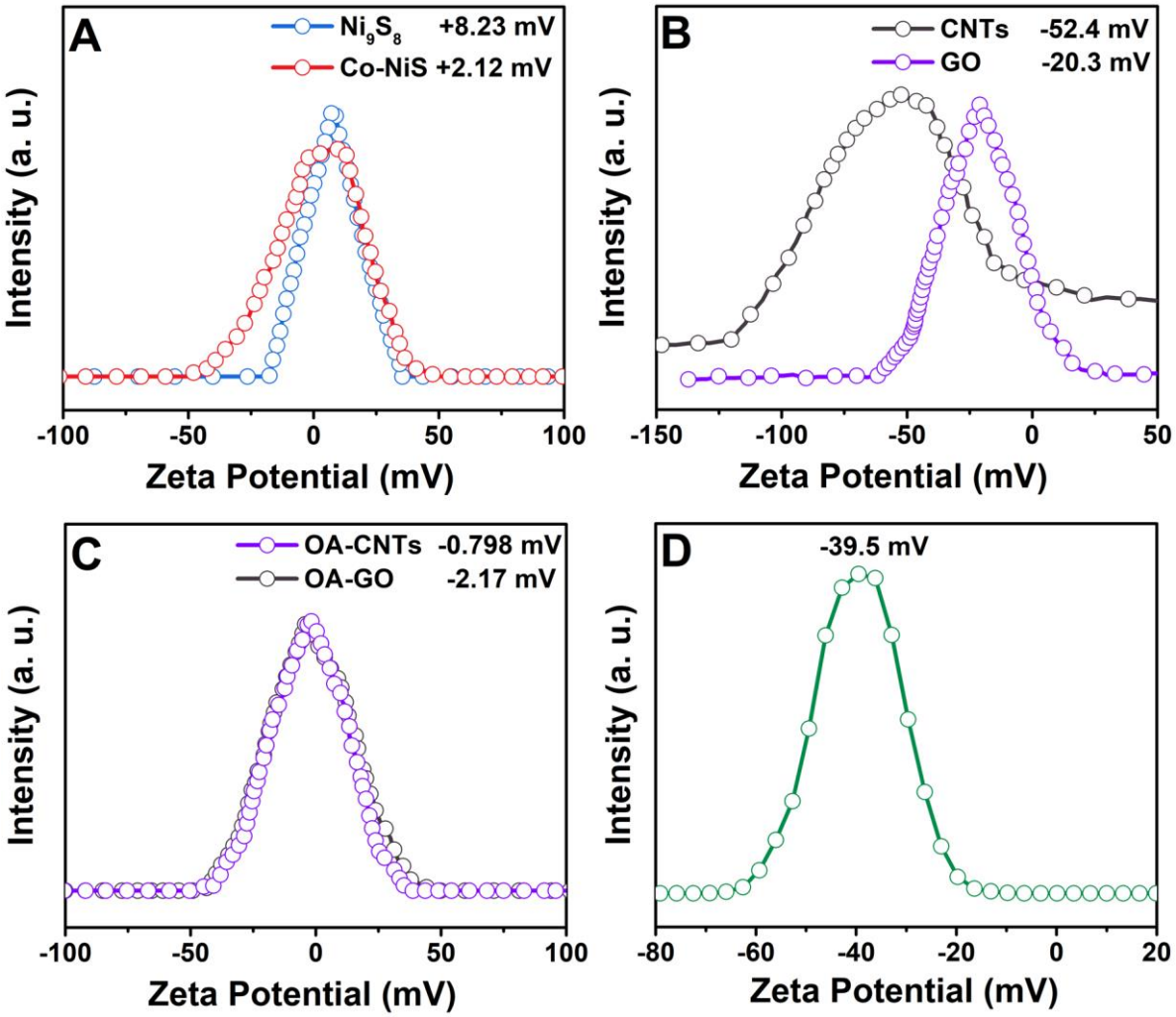

Figure S2. Zeta potentials. (A) Ni_9S_8 and Co-NiS. (B) GO and CNTs. (C) OA-GO and OA-CNTs. (D) $Ti_3C_2T_x$ MXene aqueous colloidal dispersion.

Figure S3. Optical images of of $Ti_3C_2T_x$ MXene dispersion mixed with OA (left) and OA in cyclohexane (right).

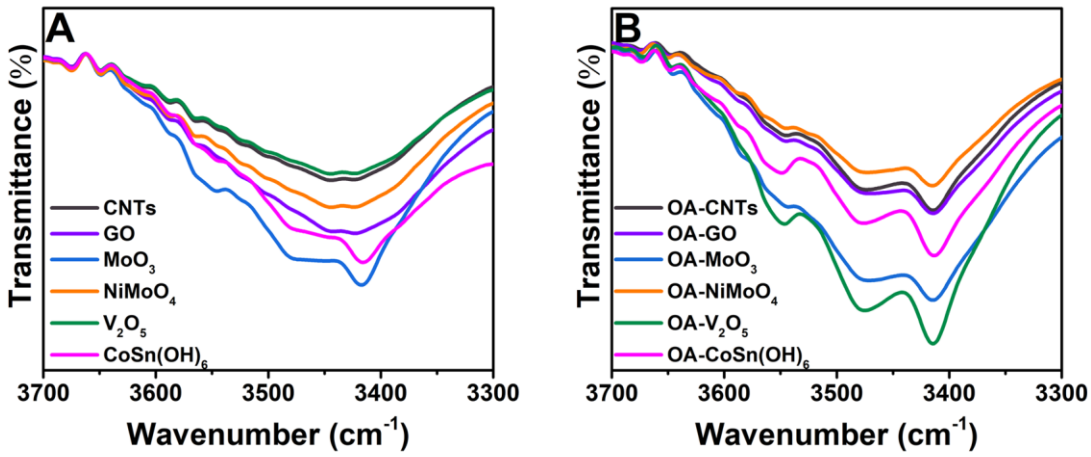

Figure S4. FT-IR spectra of the samples. (A) Samples without OA functionalization. (B) OA functionalized samples.

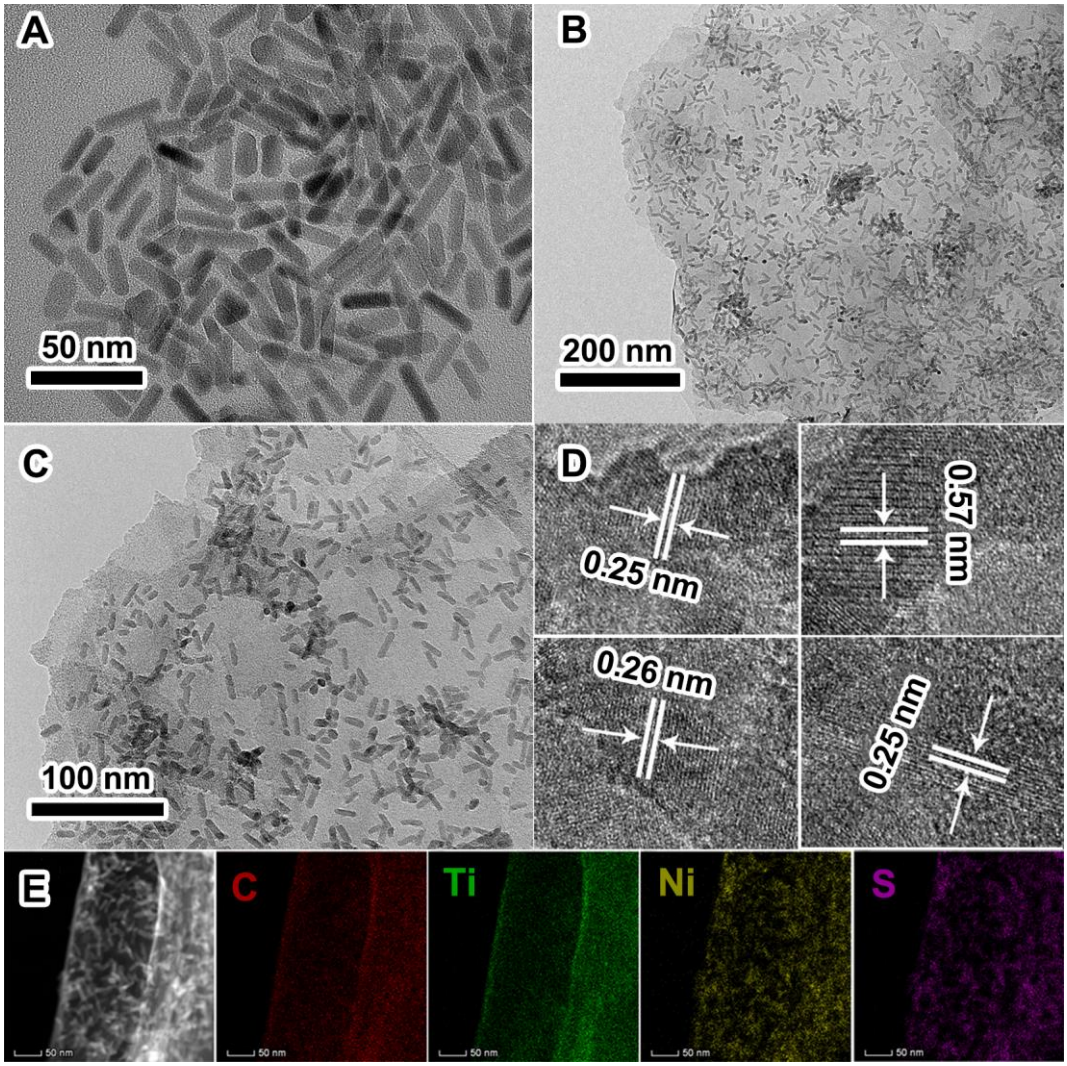

Figure S5. Morphology characterizations of the Ni_9S_8/MXene composite. (A) TEM image of pure Ni_9S_8 nanorods. (B) Low-resolution and (C) high-resolution TEM images. (D) HRTEM of Ni_9S_8/MXene. (E) EDS elemental mapping images.

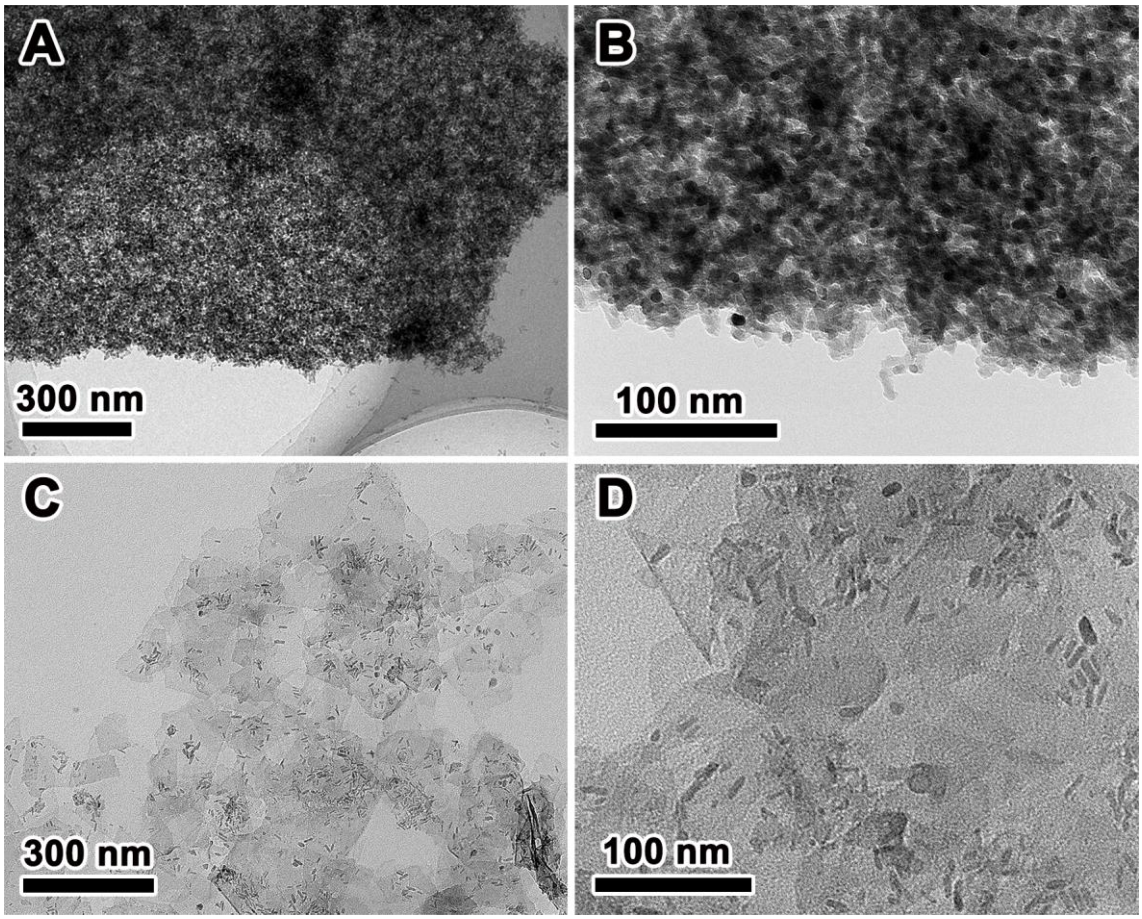

Figure S6. TEM images. (A-B) Co-NiS/MXene-5%. (C-D) Co-NiS/MXene-35%.

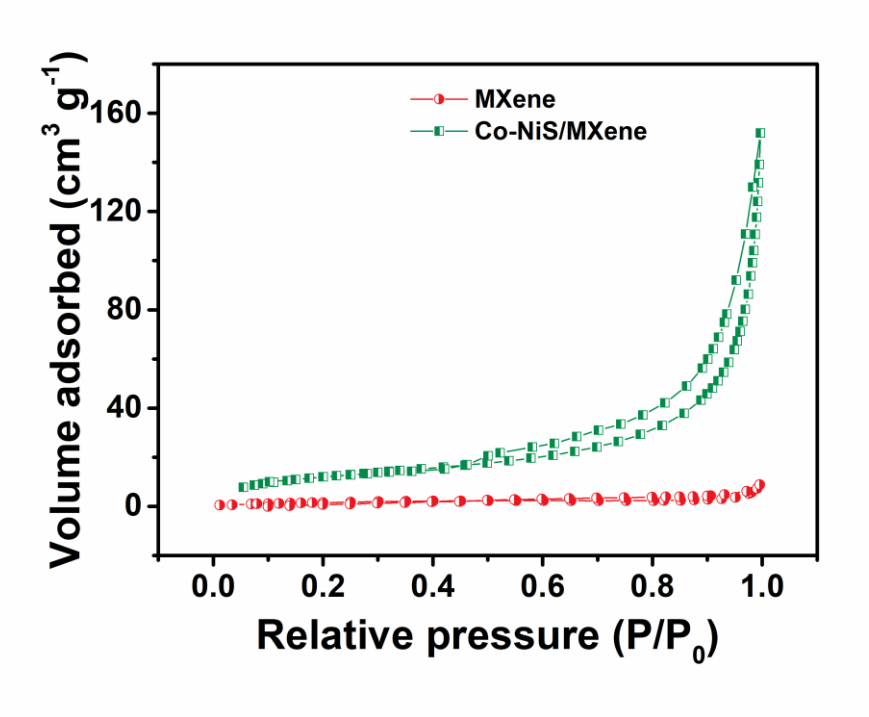

Figure S7. N_2 adsorption/desorption isotherms of MXene and Co-NiS/MXene.

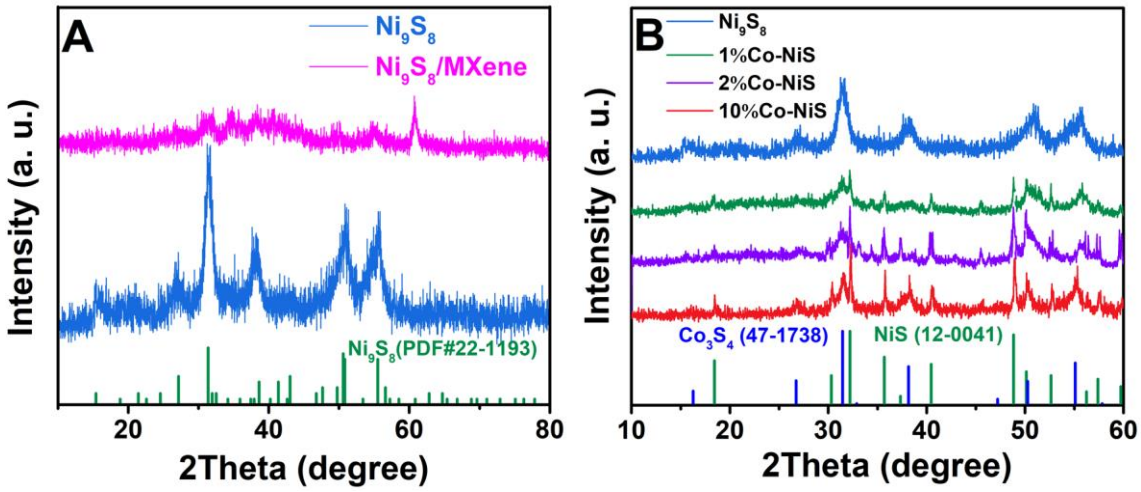

Figure S8. XRD patterns of (A) Ni_9S_8 and Ni_9S_8/MXene composite, (B) Ni_9S_8, 1%Co-NiS, 2%Co-NiS and 10%Co-NiS.

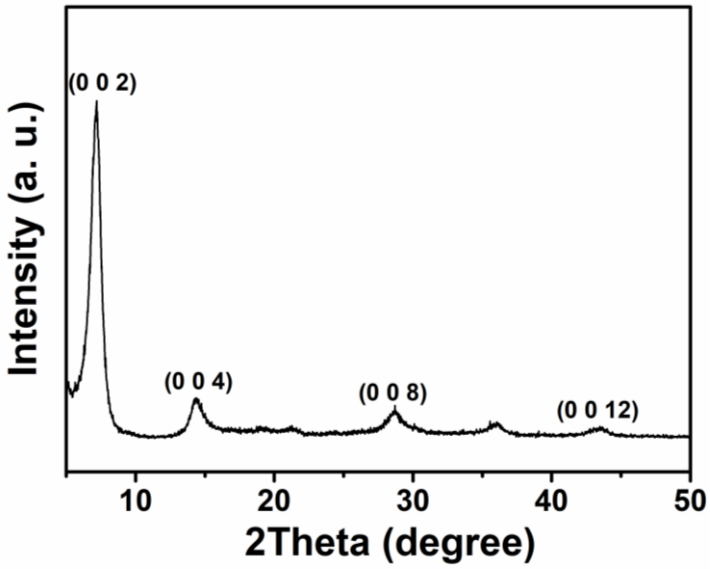

Figure S9. XRD pattern of individual $Ti_3C_2T_x$ MXene.

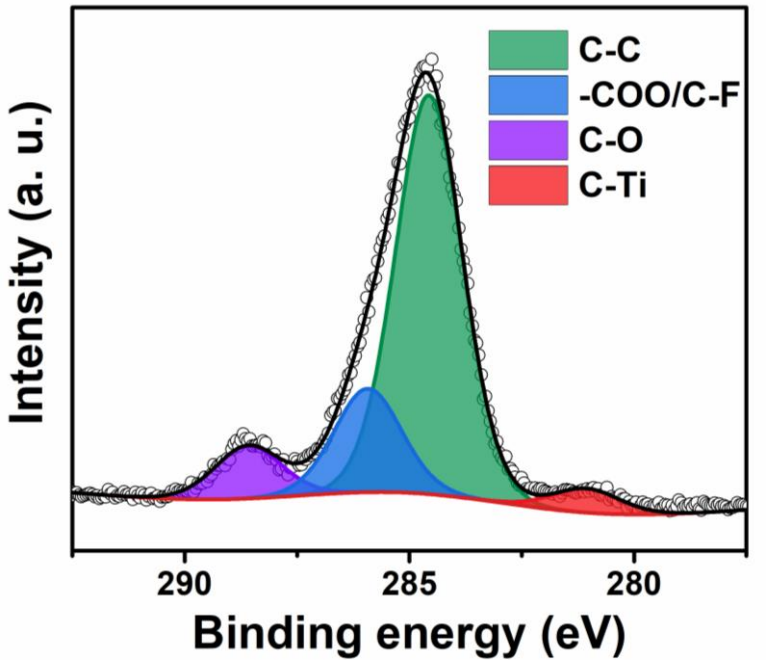

Figure S10. Core-level C 1s spectrum of the Co-NiS/MXene composite.

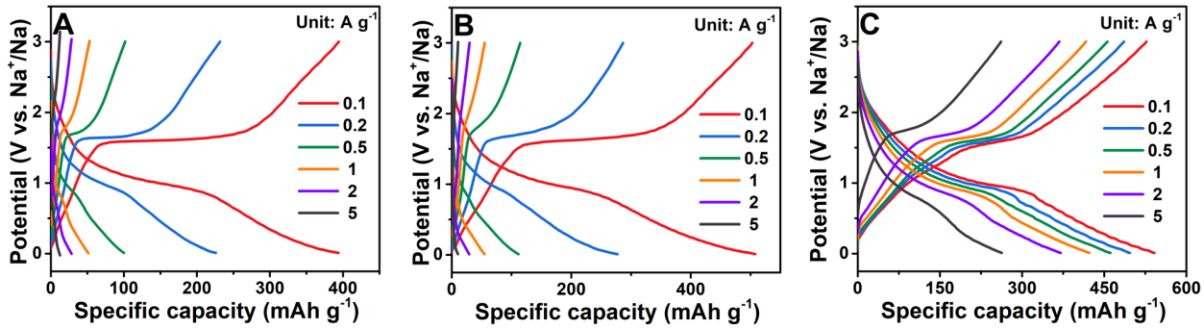

Figure S11. GCD curves for sodium ion batteries. (A) Ni_9S_8, (B) Co-NiS and (C) Co-NiS/MXene at different current densities.

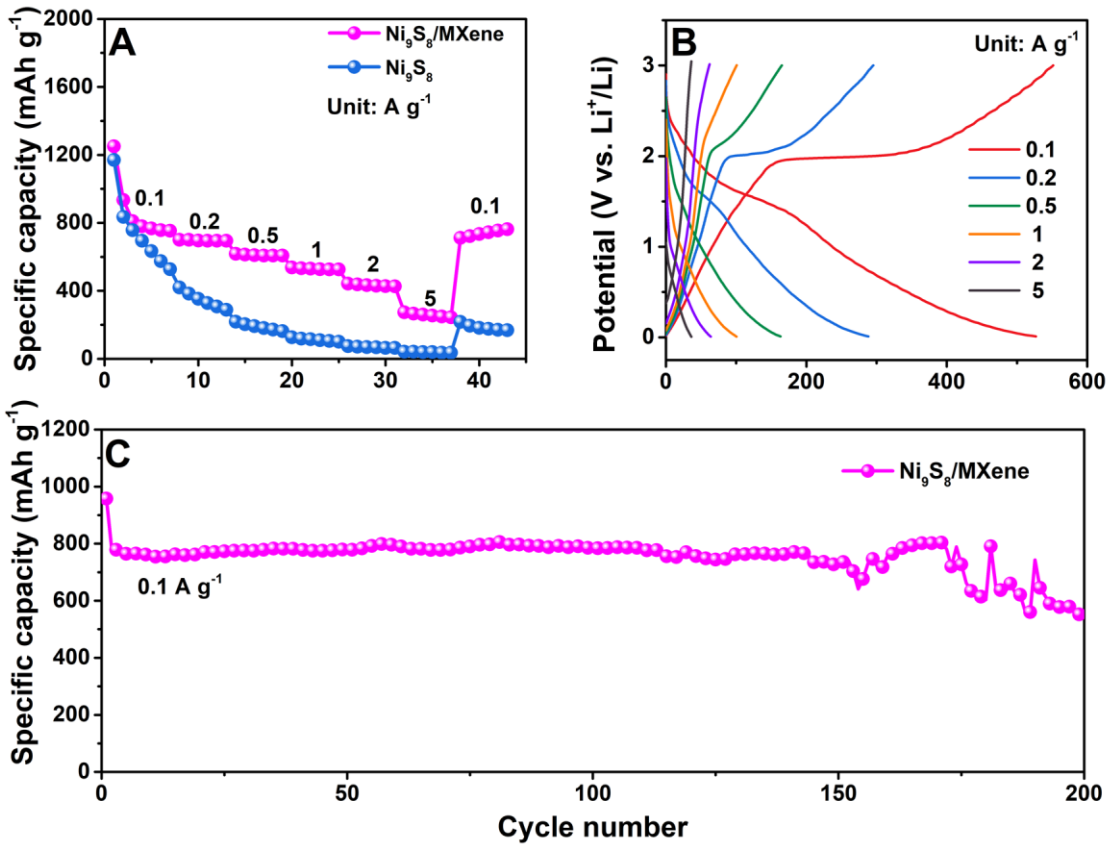

Figure S12. Electrochemical lithium storage performances. (A) Rate performance of Ni_9S_8 and Ni_9S_8/MXene. (B) GCD curves of Ni_9S_8. (B) Cycling performance of the Ni_9S_8/MXene composite at 0.1 A g^{-1}.

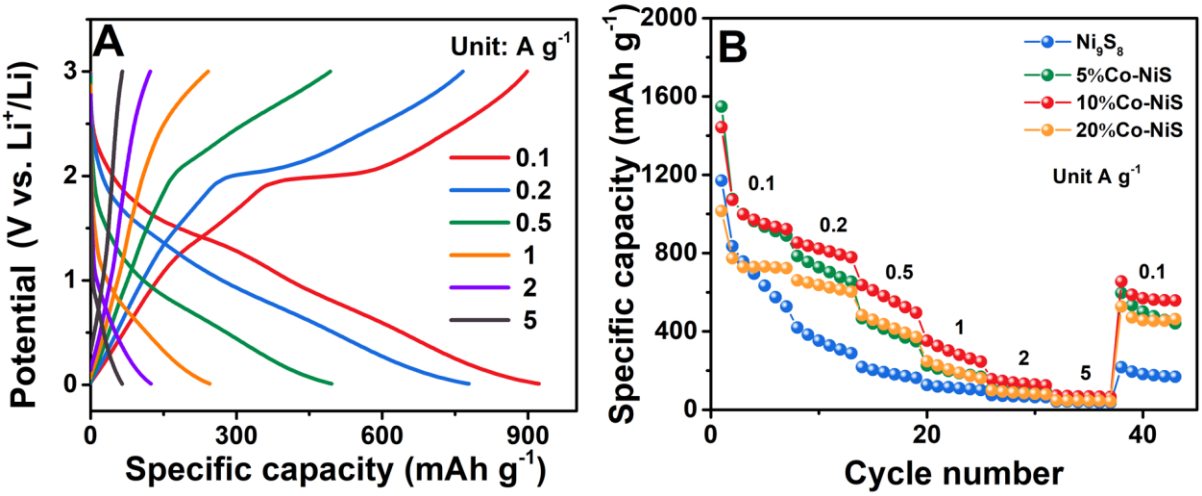

Figure S13. Electrochemical lithium storage performances of Co-NiS. (A) GCD curves at different current densities (10%Co-NiS). (B) Rate performances of the samples with different amounts of introduced Co.

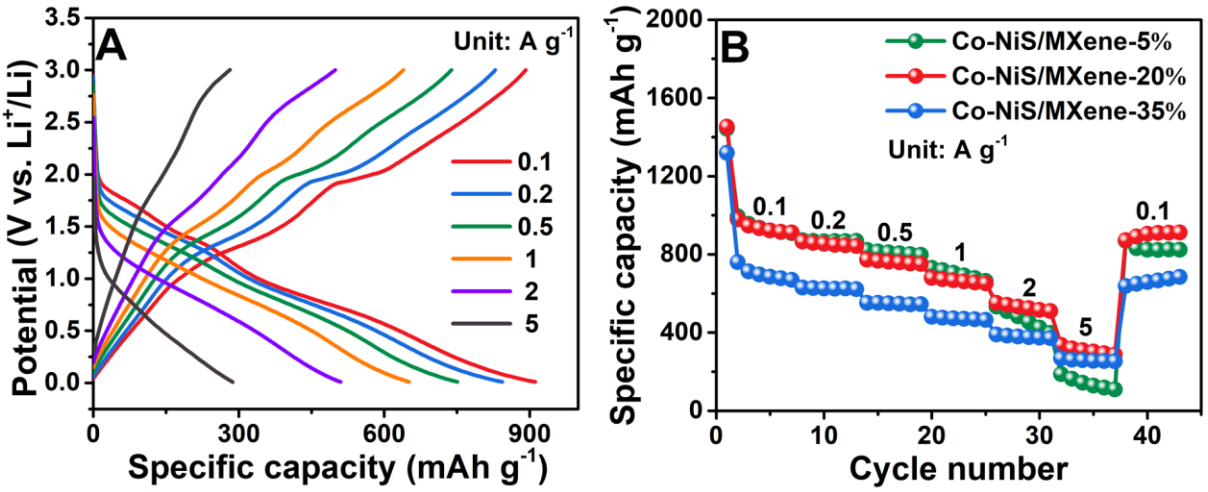

Figure S14. Electrochemical lithium storage performances of Co-NiS/MXene with different content of MXene. (A) GCD curves of the Co-NiS/MXene-20% at different current densities. (B) Specific capacities at different current densities.

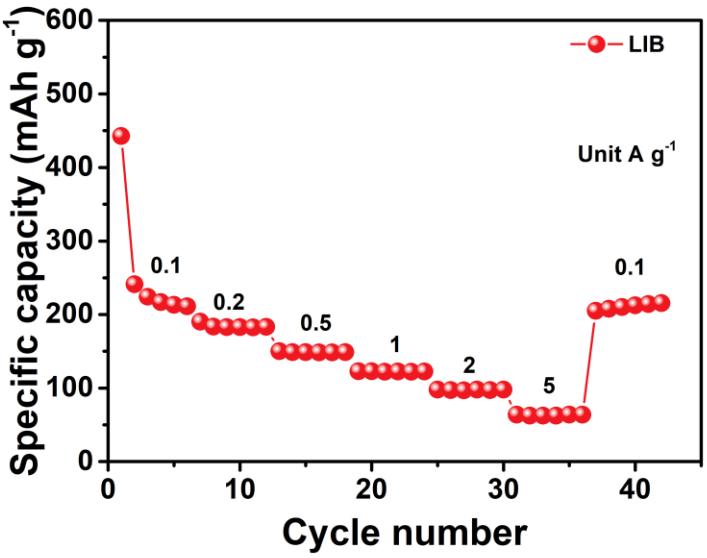

Figure S15. Rate performance of pure MXene for LIB.

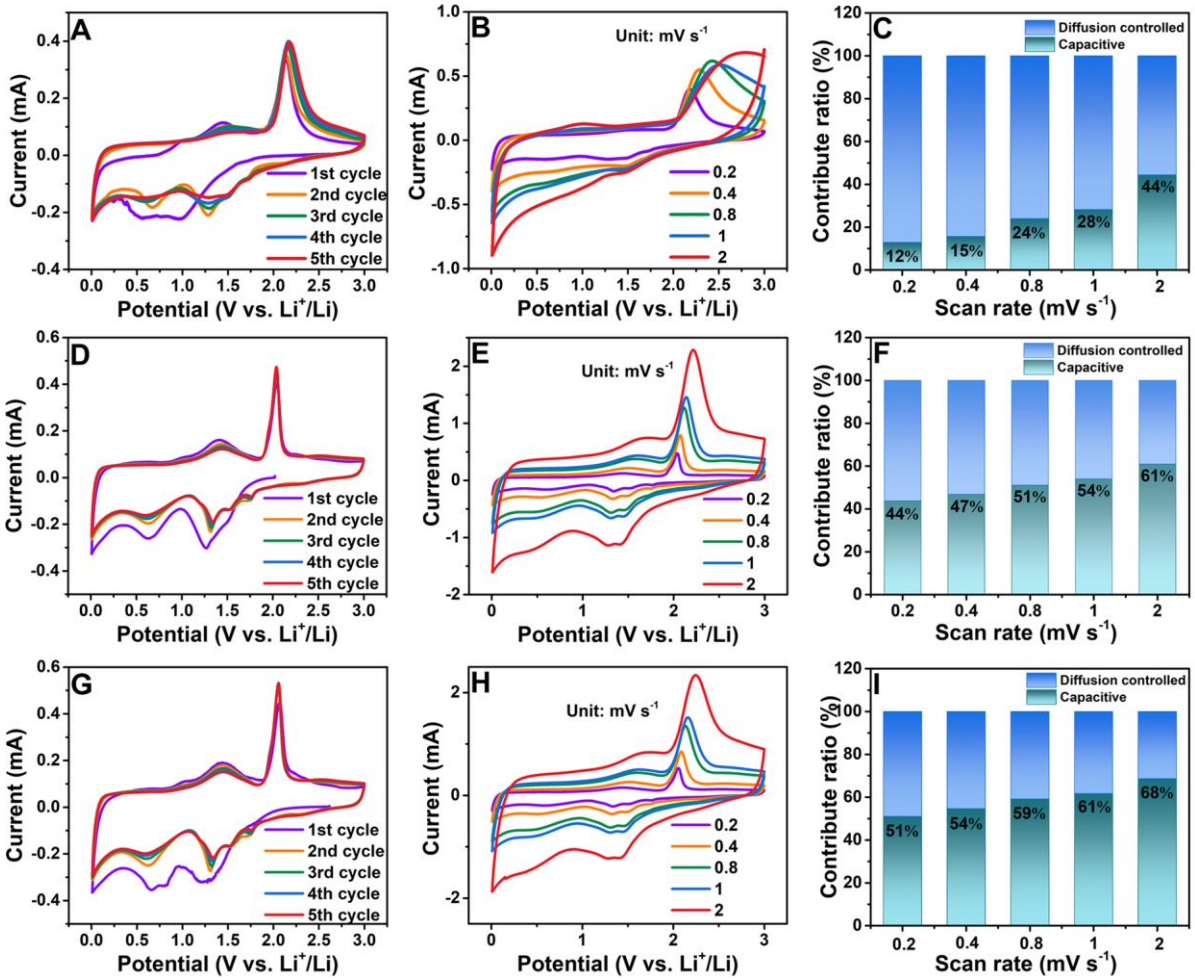

Figure S16. CV curves and capacitive contribution. (A-C) Ni_9S_8. (D-F) Ni_9S_8/MXene. (G-I) Co-NiS.

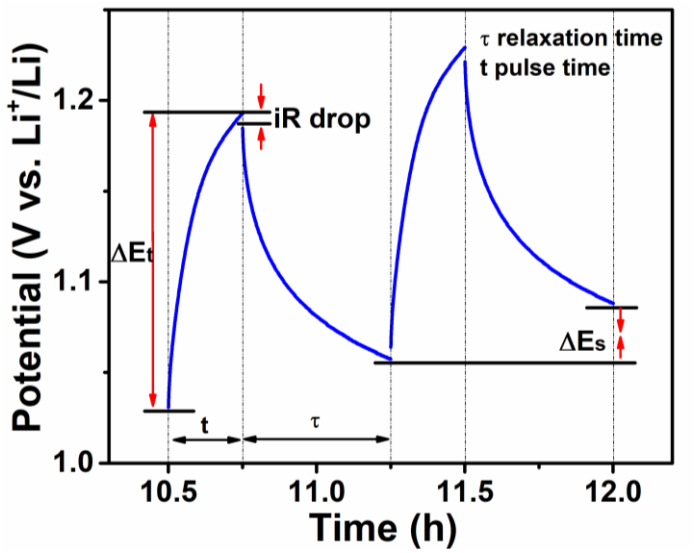

Figure S17. Enlarged GITT profiles of the Co-NiS/MXene.

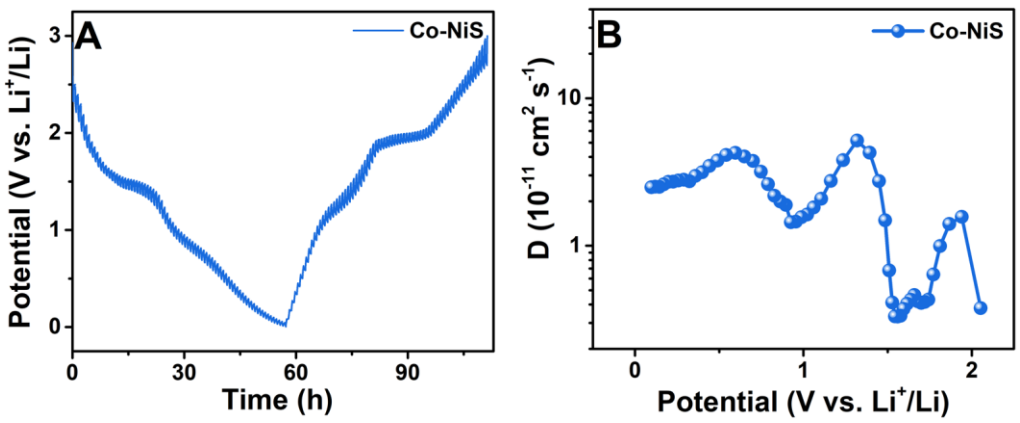

Figure S18. Electrochemical reaction kinetics analysis of Co-NiS. (A) GITT curves. (B) Diffusion coefficient (D_{Li^+}).

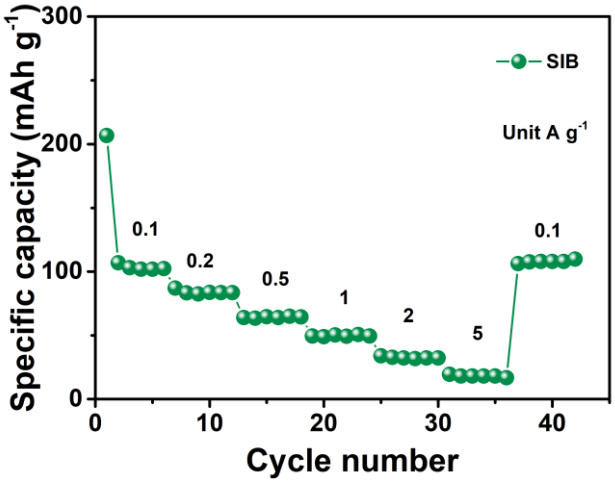

Figure S19. Rate performance of pure MXene for SIB.

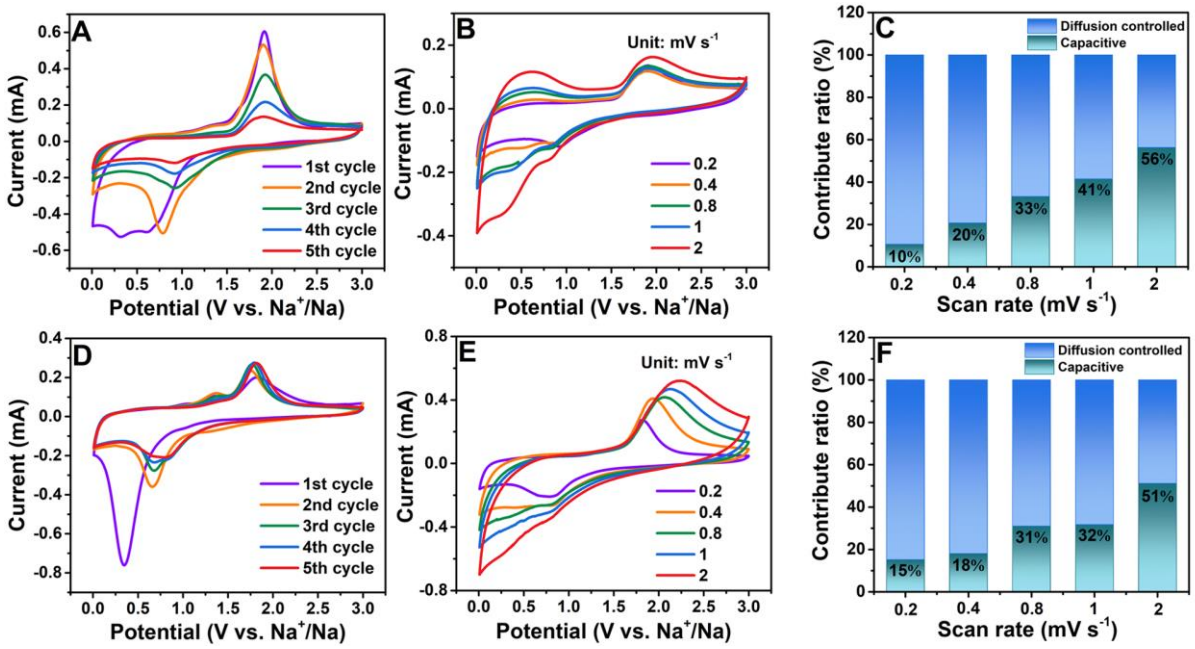

Figure S20. CV curves and capacitive contribution. (A-C) Ni_9S_8. (D-F) Co-NiS.

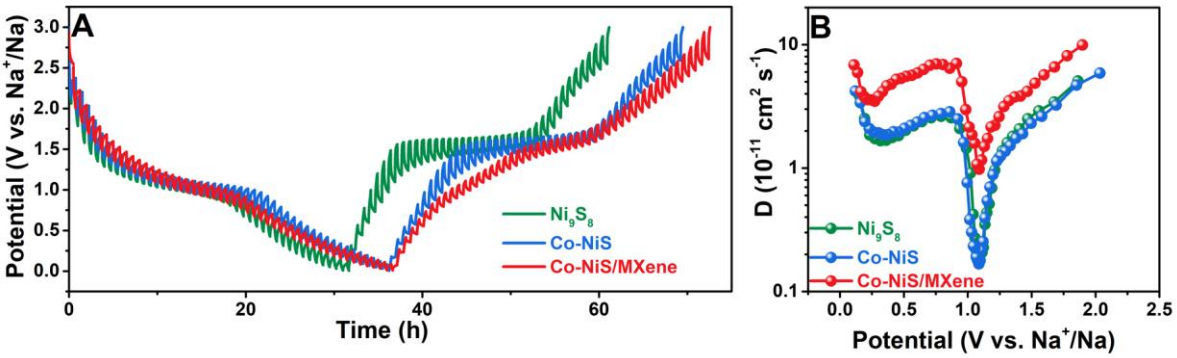

Figure S21. Electrochemical reaction kinetics analysis. (A) GITT curves. (B) Diffusion coefficient (D_{Na^+}).

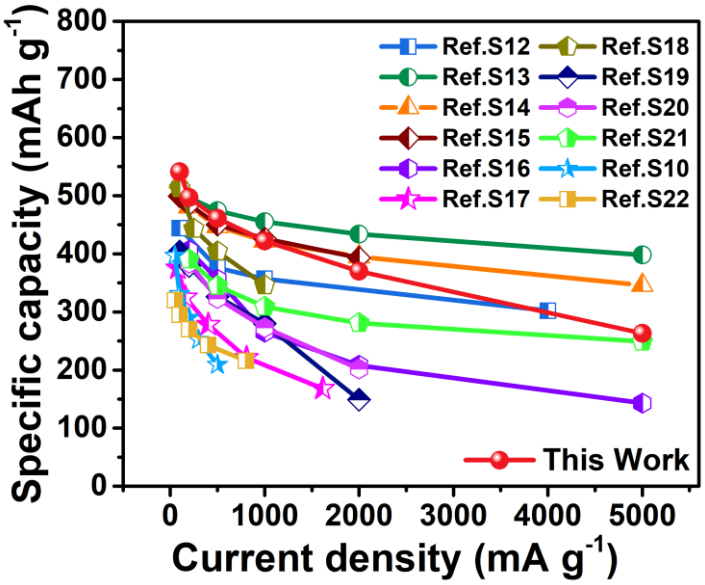

Figure S22. Comparison of the rate performance of the Co-NiS/MXene in sodium ion battery with those of the relevant materials reported recently in literature.

Table S1. Zeta potential of samples.

Materials	Ni_9S_8	Co-NiS	MXene	GO	CNTs	OA-GO	OA-CNTs
Zeta potential (mV)	8.23	2.12	-39.5	-20.3	-37.7	-2.17	-0.80

Table S2. Comparison of the rate and cycle performance performances of the Co-NiS/MXene in lithium ion battery with those of the relevant materials reported recently in literature.

Materials	Current density ($mA\ g^{-1}$)	Specific capacity ($mAh\ g^{-1}$)	Rate capability ($mAh\ g^{-1}$)	Cycling stability ($mAh\ g^{-1}$)	Refs.
Ni_2P@C	100	371	204 (1000 mA g^{-1})	398.5 (50 cycles @ 54.2 mA g^{-1})	1
Co_9S_8@C	100	704	493 (2000 mA g^{-1})	823 (200 cycles @ 100 mA g^{-1})	2
Ni_3S_2	100	689	467 (2000 mA g^{-1})	660.9 (60 cycles @ 100 mA g^{-1})	3
NS/G-10	70	834	141 (5000 mA g^{-1})	662 (200 cycles @ 70 mA g^{-1})	4
Ni_3S_2@N-G	50	815	277 (4000 mA g^{-1})	809 (150 cycles @ 50 mA g^{-1})	5
Ni_3S_2/Ni	50	299	185 (1750 mA g^{-1})	323 (100 cycles @ 170 mA g^{-1})	6
NiS@OLC	100	579	406 (4000 mA g^{-1})	546 (100 cycles @ 100 mA g^{-1})	7
NiO/NiS/Ni_3S_2	100	741	160 (3200 mA g^{-1})	499 (100 cycles @ 500 mA g^{-1})	8
NiS@NSC	100	601	446 (2000 mA g^{-1})	716 (200 cycles @ 100 mA g^{-1})	9
NiS	100	784	410 (5000 mA g^{-1})	468 (100 cycles @ 1000 mA g^{-1})	10
NiS-PPy-CNF	---	---	306 (1000 mA g^{-1})	635 (100 cycles @ 100 mA g^{-1})	11
Co-NiS/MXene	**100**	**911**	**509 (2000 mA g^{-1})**	**1120 (200 cycles @ 100 mA g^{-1})**	**This work**

Table S3. Comparison of the rate and cycle performances of the Co-NiS/MXene in sodium ion battery with those of the relevant materials reported recently in literature.

Materials	Current density ($mA\ g^{-1}$)	Specific capacity ($mAh\ g^{-1}$)	Rate capability ($mAh\ g^{-1}$)	Cycling stability ($mAh\ g^{-1}$)	Refs.
CZS	100	444	302 (4000 mA g^{-1})	294 (600 cycles @ 500 mA g^{-1})	12
NMSCHSs	100	516	398 (5000 mA g^{-1})	335 (200 cycles @ 1000 mA g^{-1})	13
MSNBs	100	524	395 (2000 mA g^{-1})	438 (100 cycles @ 200 mA g^{-1})	14
NiS/GNSs	100	499	393 (2000 mA g^{-1})	438 (100 cycles @ 200 mA g^{-1})	15
NiSx/CNT@C	200	406	208 (2000 mA g^{-1})	340 (200 cycles @ 100 mA g^{-1})	16
NiS_2-GNS	81	168	467 (1614 mA g^{-1})	313 (200 cycles @ 81 mA g^{-1})	17
NSRGO	100	513	346 (1000 mA g^{-1})	391 (50 cycles @ 100 mA g^{-1})	18
CoS/rGO	100	404	149 (1000 mA g^{-1})	277 (100 cycles @ 200 mA g^{-1})	19
CoS_2/rGO	100	384	202 (2000 mA g^{-1})	251 (150 cycles @ 500 mA g^{-1})	20
$NiSe_2$	200	390	281 (5000 mA g^{-1})	311 (100 cycles @ 100 mA g^{-1})	10
NiS_2	100	331	209 (500 mA g^{-1})	281 (60 cycles @ 100 mA g^{-1})	21
Ni_3S_2/Ni	100	295	216 (800 mA g^{-1})	348 (100 cycles @ 50 mA g^{-1})	22
Co-NiS/MXene	**100**	**541**	**422 (1000 mA g^{-1})**	**409 (100 cycles @ 100 mA g^{-1})**	**This work**

REFERENCES

(1) Zhang, R. Z.; Zhu, K. J.; Huang, J. D.; Yang, L. Y.; Li, S. T.; Wang, Z. Y.; Xie, J. R.; Wang, H.; Liu, J., Ultrafine Ni_2P Nanoparticles Embedded in One-Dimensional Carbon Skeleton Derived from Metal-Organic Frameworks Template as a High-Performance Anode for Lithium Ion Battery. *J. Alloys Compd.* **2019,** *775*, 490-497.

(2) Wang, W.; Zeng, P.; Li, J.; Zhao, Y.; Chen, M.; Shao, J.; Fang, Z., Ultrathin Nanosheets Assembled Hierarchical Co/NiS_x@C Hollow Spheres for Reversible Lithium Storage. *ACS Appl. Nano Mater.* **2018,** *1*, 3435-3445.

(3) Wang, Y.; Niu, Y.; Li, C. M., The Effect of the Morphologies of Ni_3S_2 Anodes on the Performance of Lithium-Ion Batteries. *ChemistrySelect* **2017,** *2*, 4445-4451.

(4) AbdelHamid, A. A.; Yang, X.; Yang, J.; Chen, X.; Ying, J. Y., Graphene-Wrapped Nickel Sulfide Nanoprisms with Improved Performance for Li-Ion Battery Anodes and Supercapacitors. *Nano Energy* **2016,** *26*, 425-437.

(5) Zhu, J.; Li, Y.; Kang, S.; Wei, X.-L.; Shen, P. K., One-Step Synthesis of Ni_3S_2 Nanoparticles Wrapped with *in Situ* Generated Nitrogen-Self-Doped Graphene Sheets with Highly Improved Electrochemical Properties in Li-Ion Batteries. *J. Mater. Chem. A* **2014,** *2*, 3142-3147.

(6) Su, C.-W.; Li, J.-M.; Yang, W.; Guo, J.-M., Electrodeposition of Ni_3S_2/Ni Composites as High-Performance Cathodes for Lithium Batteries. *J. Phys. Chem. C* **2013,** *118*, 767-773.

(7) Han, D.; Xiao, N.; Liu, B.; Song, G.; Ding, J., One-Pot Synthesis of Core/Shell-Structured NiS@Onion-Like Carbon Nanocapsule as a High-Performance Anode Material for Lithium-Ion Batteries. *Mater. Lett.* **2017,** *196*, 119-122.

(8) Wu, X.; Li, S.; Xu, Y.; Wang, B.; Liu, J.; Yu, M., Hierarchical Heterostructures of NiO Nanosheet Arrays Grown on Pine Twig-Like β-NiS@Ni_3S_2 Frameworks as Free-Standing

Integrated Anode for High-Performance Lithium-Ion Batteries. *Chem. Eng. J.* **2019,** *356*, 245-254.

(9) Dong, X.; Deng, Z.-P.; Huo, L.-H.; Zhang, X.-F.; Gao, S., Large-Scale Synthesis of NiS@N and S Co-Doped Carbon Mesoporous Tubule as High Performance Anode for Lithium-Ion Battery. *J. Alloys Compd.* **2019,** *788*, 984-992.

(10) Fan, H.; Yu, H.; Wu, X.; Zhang, Y.; Luo, Z.; Wang, H.; Guo, Y.; Madhavi, S.; Yan, Q., Controllable Preparation of Square Nickel Chalcogenide (NiS and $NiSe_2$) Nanoplates for Superior Li/Na Ion Storage Properties. *ACS Appl. Mater. Interfaces* **2016,** *8*, 25261-25267.

(11) Li, X.; Chen, Y.; Zou, J.; Zeng, X.; Zhou, L.; Huang, H., Stable Freestanding Li-ion Battery Cathodes by *in Situ* Conformal Coating of Conducting Polypyrrole on NiS-Carbon Nanofiber Films. *J. Power Sources* **2016,** *331*, 360-365.

(12) Ren, W.-F.; Zhou, Y.; Li, J.-T.; Huang, L.; Sun, S.-G., Si Anode for Next-Generation Lithium-Ion Battery. *Curr. Opin. Electrochem.* **2019,** *18*, 46-54.

(13) Xie, H.; Chen, M.; Wu, L., Hierarchical Nanostructured NiS/MoS_2/C Composite Hollow Spheres for High Performance Sodium-Ion Storage Performance. *ACS Appl. Mater. Interfaces* **2019,** *11*, 41222-41228.

(14) Wang, X.; Chen, Y.; Fang, Y.; Zhang, J.; Gao, S.; Lou, X. W. D., Synthesis of Cobalt Sulfide Multi-Shelled Nanoboxes with Precisely Controlled Two to Five Shells for Sodium-Ion Batteries. *Angew. Chem. Int. Ed.* **2019,** *58*, 2675-2679.

(15) Wang, J.; Cao, D.; Yang, G.; Yang, Y.; Wang, H., Synthesis of NiS/Carbon Composites as Anodes for High-Performance Sodium-Ion Batteries. *J. Solid State Electr.* **2017,** *21*, 3047-3055.

(16) Zhao, F.; Gong, Q.; Traynor, B.; Zhang, D.; Li, J.; Ye, H.; Chen, F.; Han, N.; Wang, Y.; Sun, X.; Li, Y., Stabilizing Nickel Sulfide Nanoparticles with an Ultrathin Carbon Layer

for Improved Cycling Performance in Sodium Ion Batteries. *Nano Res.* **2016,** *9*, 3162-3170.

(17) Wang, T.; Hu, P.; Zhang, C.; Du, H.; Zhang, Z.; Wang, X.; Chen, S.; Xiong, J.; Cui, G., Nickel Disulfide-Graphene Nanosheets Composites with Improved Electrochemical Performance for Sodium Ion Battery. *ACS Appl. Mater. Interfaces* **2016,** *8*, 7811-7817.

(18) Qin, W.; Chen, T.; Lu, T.; Chua, D. H. C.; Pan, L., Layered Nickel Sulfide-Reduced Graphene Oxide Composites Synthesized *via* Microwave-Assisted Method as High Performance Anode Materials of Sodium-Ion Batteries. *J. Power Sources* **2016,** *302*, 202-209.

(19) Zhu, X.; Jiang, X.; Liu, X.; Xiao, L.; Ai, X.; Yang, H.; Cao, Y., Amorphous CoS Nanoparticle/Reduced Graphene Oxide Composite as High-Performance Anode Material for Sodium-Ion Batteries. *Ceram. Int.* **2017,** *43*, 9630-9635.

(20) Li, Z.; Feng, W.; Lin, Y.; Liu, X.; Fei, H., Flaky CoS_2 and Graphene Nanocomposite Anode Materials for Sodium-Ion Batteries with Improved Performance. *RSC Adv.* **2016,** *6*, 70632-70637.

(21) Zhu, K. J.; Liu, G.; Wang, Y. J.; Liu, J.; Li, S. T.; Yang, L. Y.; Liu, S. L.; Wang, H.; Xie, T., Metal-Organic Frameworks Derived Novel Hierarchical Durian-Like Nickel Sulfide (NiS_2) as an Anode Material for High-Performance Sodium-Ion Batteries. *Mater. Lett*. **2017,** *197*, 180-183.

(22) Song, X.; Li, X.; Bai, Z.; Yan, B.; Li, D.; Sun, X., Morphology-Dependent Performance of Nanostructured Ni_3S_2/Ni Anode Electrodes for High Performance Sodium Ion Batteries. *Nano Energy* **2016,** *26*, 533-540.